Biosensors and Bioelectronics 201 (2022) 113956

Contents lists available at ScienceDirect

Biosensors and Bioelectronics

journal homepage: www.elsevier.com/locate/bios

Bio-electron transfer modulated localized surface plasmon resonance biosensing with charge density monitoring

Zetao Chen [a], Fenni Zhang [a], Yaru Li [a], Jianzhen Shan [b], Yanli Lu [a,c,*], Qingjun Liu [a,c]

[a] Biosensor National Special Laboratory, Key Laboratory for Biomedical Engineering of Education Ministry, Department of Biomedical Engineering, Zhejiang University, Hangzhou, 310027, PR China
[b] The First Affiliated Hospital, Zhejiang University School of Medicine, Hangzhou, 310003, PR China
[c] Collaborative Innovation Center of TCM Health Management, Fujian University of Traditional Chinese Medicine, Fuzhou, 350108, PR China

ARTICLE INFO

Keywords:
Localized surface plasmon resonance (LSPR)
Electron transfer
Bioreaction
Charge density
Biosensor

ABSTRACT

The analysis of reactant at different regions of the bioreaction interface is significant for the study on the influence of interface condition on bioreaction. In this study, we proposed a localized surface plasmon resonance (LSPR) biosensing platform for local charge density monitoring and corresponding analytes detection based on the bio-electron transfer modulation of plasmon resonance. Core-shell nanocomposites of polyaniline coated gold nanoparticles were synthesized for the enhanced sensitivity of plasmon resonance to applied electric potential. Tin-doped indium oxide (ITO) substrates modified with the nanocomposites were used as LSPR chip for optical and electrochemical measurements simultaneously. The charge sensitivity of LSPR was verified with external electric potential modulation theoretically and experimentally. Through layer-by-layer self-assembly immobilization of glucose oxidase (GOD) on the LSPR chips, the charge transfer monitoring during the bioreaction of glucose catalysis was further demonstrated based on the bio-electron transfer modulation of LSPR. By equivalent circuit method, the charge density of the LSPR chip were detected with optical extinction peak shifts, and the limit of detection was about 0.51 μC/cm^2. This bio-electron transfer modulated LSPR provides a promising approach for the detection of spatial charge densities and the evaluation of bioreaction substances at different region of single chip.

1. Introduction

When light source with specific wavelength illuminated on plasmonic nanoparticles, an electromagnetic field occurs that driving the collective oscillations of nanoparticles' free electrons into resonance, which leads to strong extinction (absorption and scatterings) of photon energy, resulting in localized surface plasmon resonance (LSPR) (Mayer and Hafner, 2011; Nehl and Hafner, 2008; Xu and Geng, 2021). At the wavelength corresponding to the resonant frequency, the optical extinction peak of nanoparticles could be observed, which is related to the refractive index of nanoparticle (Cortie and McDonagh, 2011). Due to the ultrasensitivity to surrounding refractive index changes, LSPR is often used for rapid, real-time, and label-free biochemical sensing (Jackman et al., 2017; Loiseau et al., 2019). Therefore, based on the mechanism of optical extinction peak shifts, LSPR sensors were sensitive to target analytes which can combine to recognition materials immobilized on nanoparticles and lead a change in refractive index.

To further improve the detection sensitivity, electrochemical methods had been coupled with LSPR detections, which could provide additional sensing information during the optical measurements (Li et al., 2018; Zhang et al., 2015). Based on the electrochemical coupling, external electric potentials modulated LSPR had been studied for the detection of refractive index (Ran et al., 2018). During the detection, noble metal nanoparticles modified tin-doped indium oxide (ITO) transparent substrates were treated as LSPR chips for the simultaneous electric potential applying and optical extinction measurement. In order to improve the sensitivity, nanoparticles modified by conductive polymers, such as polyaniline, polypyrrole, or polythiophene, are sometimes used instead of pure nanoparticles (Jeon et al., 2016). Under the influence of electromagnetic fields generated by external applied potentials, the free electrons distribution of metal nanoparticles was changed and the refractive index was affected, which resulted in optical extinction

* Corresponding author. Biosensor National Special Laboratory, Key Laboratory for Biomedical Engineering of Education Ministry, Department of Biomedical Engineering, Zhejiang University, Hangzhou, 310027, PR China.
E-mail address: yanlilu@zju.edu.cn (Y. Lu).

https://doi.org/10.1016/j.bios.2021.113956
Received 8 August 2021; Received in revised form 15 November 2021; Accepted 30 December 2021
Available online 4 January 2022

peak shifts (Kitajima et al., 2021). Due to the sensitivity to electric potentials and the ease of potential control implementation, this electric potential modulated LSPR phenomenon could be used for the evaluation of electron densities.

Substrates such as ion selective membranes or electrodes immobilized with biosensitive materials often used as biochips for biosensing applications. Enzyme electrodes, as the earliest biosensors, were fabricated for specifically detection and functioned by combining the electrochemical procedure with immobilized enzyme activity (Mano, 2019; Updike and Hicks, 1967). During the detection period using enzyme electrodes, electron transfers reflected on electric currents were observed. Through the circuit formed by electrolyte and electrodes, in the electrochemical detection, electron density of the electrode was increased due to the electron transfers of enzymatic catalysis such as glucose oxidase (GOD) catalyzing glucose oxidization (Freguia et al., 2012; Zhong et al., 2018). Inspired by the electron enrichment of enzymatic catalysis process, if this bio-electron transfer could be used for the modulation of LSPR, charge densities at different region of the reaction interface can be monitored based on the spot size of incident light. Furthermore, the substances involved in the bioreaction can be evaluated correspondingly with the charge density. The analysis of reactant at different regions of the interface is significant for the study on the influence of interface conditions on biological reaction.

In this paper, based on the bio-electron transfer modulation of LSPR, a biosensing platform was constructed for local charge density monitoring and corresponding analytes detection. Firstly, the nanocomposites of conductive polyaniline coated gold nanoparticles were synthesized for the enhancement of electric sensitivity, and the ITO substrates modified with the nanocomposites were used as LSPR chips for the electric potential modulation of plasmon resonance. Secondly, to analyze the modulation mechanism theoretically, the influences of electric potentials to optical extinction was quantitatively calculated by finite-difference time-domain (FDTD) simulation. Finally, the bioreaction of GOD catalyzing glucose were used as demonstration for the bio-electron transfer modulation of optical extinction. Through the equivalent circuit method, the mechanism enabled the detection of spatial charge density and the evaluation of bioreaction substances at different region of single chip.

2. Materials and methods

2.1. Reagents and apparatus

Chloroauric acid ($HAuCl_4$) was dissolved in deionized water with 1% (w/v) for the synthesis of gold nanoparticles (AuNPs). Trisodium citrate ($Na_3C_6H_5O_7$) was dissolved in deionized water with volume ratio of 1% (w/v) as reducing agent. Aniline, hydrochloric acid (HCl), sodium dodecyl sulfate (SDS), and ammonium persulfate ($(NH_4)_2S_2O_8$) were prepared for the synthesis of polyaniline (PANI) coated AuNPs core-shell nanocomposites (AuNPs@PANI). Dichloromethane, (3-aminopropyl) triethoxysilane (ATPES), methanol, acetone, toluene, and ethanol were prepared for cleaning and positively charging of ITO substrates. Chitosan dissolved in acetic acid and GOD dissolved in 0.01 mol/L phosphate buffer solution (PBS) were prepared for the substrates' modification and functionalization. Glucose was prepared in PBS as demonstration of bio-electron transfer for subsequent experiments. All chemical agents were purchased from Sigma-Aldrich (St. Louis, MO, USA).

Electrochemical experiments were performed on the electrochemical workstation (CHI660E, USA) while optical experiments were performed on the optical detection system consisting of a high-power deuterium tungsten composite light source (DH-MINI, Ocean Optics Inc., USA) and a spectrophotometer receptor (USB2000 plus, Ocean Optics Inc., USA). Ag/AgCl electrode was used as reference electrode, Carbon electrode was used as counter electrode and the LSPR chip was treated as working electrode during the detection. Scanning electron microscope (SEM, Philips XL-30 ESEM) and transmission electron microscope (TEM, JEM-1010) were used for morphology characterization of the substrates and nanoparticles. An ultrasonic washing machine (DS-060ST, China) was used for the cleaning of substrates. A spray pen with a nozzle diameter of 0.2 mm (MoShen, China) was used for the modification of ITO substrates with nanocomposites.

2.2. Synthesis of polyaniline coated gold nanoparticles

For the optical extinction detection and electrostatic adsorption modification, negatively charged AuNPs was synthesized through the adaption of sodium citrate reduction method (Boisselier and Astruc, 2009). The $HAuCl_4$ aqueous solution with 1% (w/v) (1 mL) added into deionized water (100 mL) was treated as base solution. After the solution was stirred and brought to boil, sodium citrate solution with 1% (w/v) (2 mL) was added. The solution was boiled under constant stirring for 2 to 3 min until the color changes were observed. After 21 min, while the solution has gradually turned purple, heating and stirring were stopped. After the solution was cooled to room temperature, centrifugation process was performed at 4 °C, 12,000 rpm for 15 min to remove excess sodium citrate. The precipitate was then dispersed with 10 mL deionized water and re-centrifuged at 4 °C, 6,000 rpm for 15 min to purify the AuNPs. The precipitate was then dispersed with 2 mL deionized water for further synthesizing.

To enhance the electrical and optical properties of AuNPs, ammonium persulfate oxidative polymerization method was adapted to synthesize PANI for the preparation of PANI coated AuNPs core-shell nanocomposites (Xu et al., 2019). For the preparation of aniline-AuNPs mixture, 40 mM SDS (0.25 mL) and the above synthesized AuNPs (0.5 mL) were added into 2 mM (1.5 mL) aniline solution. After complete mixing, 2 mM ammonium persulfate (1.5 mL) prepared in 10 mM HCl aqueous solution was added. After the solution was subjected to polymerization for 24 h, PANI was attached to the surface of AuNPs, forming the core-shell nanocomposites. After the PANI residuals was removed from the suspension solution using centrifugation, the precipitate was dispersed with 1.5 mL 3.6 mM SDS solution for further purification by repeated centrifugation. Then the purified core-shell nanocomposites of AuNPs@PANI were obtained after the precipitate was dispersed with 0.5 mL deionized water.

2.3. LSPR chips for optical and electrochemical detection

To enable the potentials' applying and recording while the optical extinction detection, ITO substrates were fabricated by physical vapor deposition (PVD) as electrodes (Helmersson et al., 2006). The carbon counter electrode and the Ag/AgCl reference electrode were modified on the ITO layer by screen printing to unify the differences between electrodes. After cleaned via ultrasonic washing, the electrodes were dried and immersed in 2% (v/v) volume ratio of APTES in toluene at 75 °C for 30 min to provide positive charges to their surface. The charged electrodes were then washed to remove excessive organic solvent and heated at 110 °C for 15 min to stabilize the charges. Afterwards, the core-shell nanocomposites were sprayed to the surface of the positively charged electrodes with an injection pressure of 18 psi and a spraying distance of 6 cm to ensure the consistency. Through electrostatic adsorption, the electrodes were modified with the nanocomposites and treated as LSPR chips for optical extinction study. To enhance the conductivity of PANI, the LSPR chips were immersed in 0.2 mol/L HCl solution for 1 h for the protonation of PANI coated on AuNPs.

For the study of bio-electron transfer of enzymatic catalysis, the LSPR chips were functionally modified with GOD via drop casting. The chitosan solution was prepared in acetic acid at 0.5% (w/v). The GOD solution was prepared with 8 mg/mL in 0.01 mol/L PBS. Afterwards, the GOD solution was mixed with the chitosan solution at a volume ratio of 1:1 for the steady immobilization of GOD. After the nanocomposites of AuNPs coated with PANI layers were sprayed to the surface of ITO substrates, 10 μL chitosan-GOD solution was immobilized on the LSPR

chips via chitosan adsorption. Thereby, the LSPR chips were prepared for optical and electrochemical measurements.

2.4. Modulation of LSPR with applied potentials

FDTD simulation on the nanocomposites was performed to clarify the mechanism of potential modulated LSPR. The electromagnetic field distribution and the optical extinction spectra of the nanocomposites were calculated and analyzed as a theoretical guide for the effects of electric potential on LSPR. A spherical structure was constructed as model of the nanocomposite which was illuminated by a plane wave source with an electric field amplitude of 1 V/m. Based on the relationship between refractive indices and electric potentials (Nishi et al., 2015), the refractive indices of AuNPs and PANI with different applied potentials were calculated for the quantitative simulation of potential modulated plasmon resonance.

The electric sensitivity experiments with LSPR chips were performed to explore the modulation of optical extinction via applied electric potentials. The chips were plugged into a quartz cuvette which was fixed in a 3D printing structure on optical platform for the optical extinction spectra recording whilst electric potentials were applied. Optical extinction spectra in visible light were recorded by a spectrophotometer with 0.38 nm optical path. Electric potentials applied on LSPR chips were provided by electrochemical workstation. During the detections, the applied potential range was set at 0 V to 0.6 V with an interval of 0.2 V. Electrolyte in the quartz cuvette was 0.01 mol/L PBS. All the measurements were performed under the same conditions.

2.5. Charge density monitoring with bio-electron transfer modulated LSPR

The bioreaction of GOD catalyzing glucose was utilized for the study of bio-electron transfer modulation on LSPR. Based on the GOD immobilized LSPR chip, the optical extinction peak shift was measured with glucose concentration of 50 mmol/L. To ensure the extinction peak shift was caused by the bio-electron transfer of the enzymatic catalysis reaction, LSPR chip without the immobilization of GOD was tested at the same condition as comparison. Afterwards, the extinction peak shifts of GOD immobilized LSPR chip were measured with glucose concentration ranged from 10 mmol/L to 50 mmol/L to explorer their linearity. To calculate the charge density of the LSPR chip, open circuit potentials of the chip were detected at different glucose concentrations, and the equivalent circuit method was used to obtain the equivalent capacitance of the layered structure based on the electrochemical impedance spectroscopy of GOD immobilized LSPR chip. Additionally, LSPR chip with multiple regions were prepared by mask method for the simulation of different charge densities at one chip. Through the detection of these regions, spatial charge densities were calculated and the corresponding analytes were evaluated.

3. Results and discussion

3.1. Principle of charge density detection

In LSPR, the optical extinction peak shift represents the change of refractive index of the plasmon nanostructure. Changes in shape, size, and status of the material cause the varies of refractive index. While the plasmon nanostructure was under the illumination of excitation light, surface electrons of the nanostructure are active. With the stimulus of external applied electric potential, the distribution of the electrons will change and lead the shifts of optical extinction peak. As illustrated in Fig. 1A, the synthesized gold nanocomposites were modified onto the ITO substrates forming LSPR chips for the electric potential modulation on plasmon resonance illustrating the charge sensitivity.

Electron transfers are existed in bioreactions such as enzymatic catalysis. By immobilizing the enzyme on the plasmon nanostructure, the transferred electrons generated in the catalytic process will be enriched on the surface of the nanostructure, which affects the distribution of the surface electrons leading the refractive index changes of the nanostructure. In the spectrum, it is the shift of optical extinction peak. Taking GOD catalyzing glucose as demonstration, the GOD was immobilized on the LSPR chip, and the layered structure was showed in Fig. 1B. In the existence of molecular oxygen, aldehyde group of glucose is oxidized to carboxyl of gluconic acid by GOD and the generated electrons are directly transferred to the nanocomposite (Fig. 1C). Under the effects of electromagnetic field caused by incident light and electrons from enzymatic catalysis, the distribution of electrons on AuNPs@PANI was changed and caused the peak shifts of plasmon extinction.

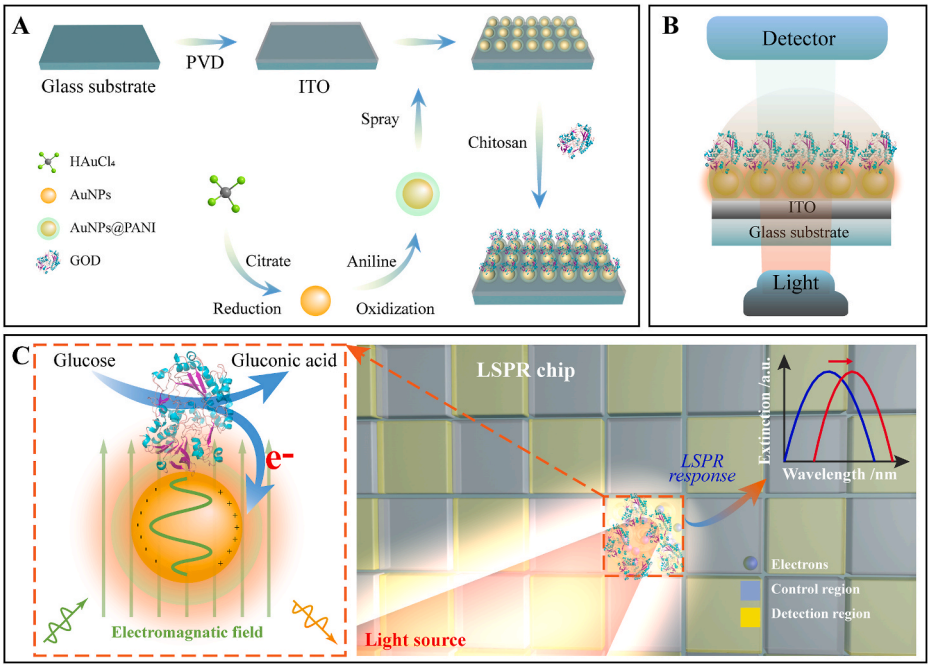

Fig. 1. The development of bio-electron transfers based LSPR biosensing platform with the monitoring of charge density. (A) Fabrication process of the LSPR chip. (B) The layered structure of LSPR chip and the detection strategy. (C) Principle of the charge density monitoring: electrons produced from the GOD catalyzing glucose were transferred to the nanocomposites of LSPR chip, and the electron distribution changes of the nanocomposite leading the shift of plasmon resonant wavelength was used for the calculation of charge density.

Through the open circuit potentials and the equivalent circuit method, the charge density can be calculated with glucose concentrations and the optical extinction peak shifts. By detecting charge densities at different regions of the LSPR chip, the detection of spatial charge density and the evaluation of corresponding glucose concentration can be realized.

3.2. Polyaniline coated gold nanoparticles on LSPR chip

The synthesis of PANI coated AuNPs core-shell nanocomposites and the modification of ITO substrates were verified by optical spectra and morphological characterizations. The optical extinction spectra of pure PANI, AuNPs, and AuNPs@PANI were measured for the difference comparison between nanocomposites and bare nanoparticles (Fig. 2A). The optical extinction peak of AuNPs@PANI nanocomposites at about 810 nm was almost the same as pure PANI solution. It means that the optical properties of PANI were kept stable under the coating process. However, because of the enlarged gap of the PANI coating layers, the optical extinction peak of AuNPs from the nanocomposites had about 5 nm red shift compared to bare AuNPs. From the TEM image, the core-shell nanostructure of PANI coated AuNPs was observed with a more uniformed distribution (Fig. 2B) than bare AuNPs (inset of Fig. 2B). With the scale of the images, we can get that the average thickness of the PANI layer was about 20 nm to 25 nm, and the average diameter of AuNPs was about 40 nm.

By spray coating, the nanocomposites of AuNPs@PANI were modified on the surface of ITO substrates, and the two characteristic peaks were observed on the optical spectrum (Fig. S1). After the immobilization of GOD, the optical extinction intensity was enlarged for the GOD increased the light blocking. From the electrochemical impedance spectroscopy for each modification steps of the LSPR chip, the impedance is decreased after the modification of nanocomposites and increased after the immobilization of GOD indicating the successfully modification of LSPR chip (Fig. 2C). As showed in Fig. 2D, the core-shell nanostructures were observed on the LSPR chip through SEM, and the distribution of the nanocomposites was relatively uniform compared to bare AuNPs modified ITO substrates (Fig. S2). Therefore, the nanocomposites modified transparent ITO substrates were treated as LSPR chips for optical and electrochemical measurements simultaneously, which could provide stable spectra during the detections. Furthermore, the energy dispersive spectrometer (EDS) analysis showed the surface elements of LSPR chip indicating the nanocomposites of AuNPs@PANI were successfully modified (Fig. S3).

The PANI layer thickness, nanoparticle diameter, and distance between enzyme and PANI layer are factors that affecting the detection sensitivity and the LSPR characteristics. Based on the theoretical calculation with different thickness of PANI layers, the thickness of 20 nm–25 nm of the PANI layer was optimized and suitable in our situation for the construction of LSPR chip, improving the stability and the sensibility. Based on the theoretical calculation with different AuNPs diameters, a relatively moderate nanoparticle size such as 40 nm was optimized and chosen during the synthesis process. In addition, the distance between enzyme and PANI is depended on the density of GOD and chitosan. A smaller density of GOD leads a bigger distance between enzyme and PANI layer. Compared to physical adsorption method for the immobilization of enzyme on the PANI layer, the covalent binding was more controllable and the distance can be further optimized, leading a improving in the detection sensitivity. However, suitable cross-linker for covalent binding is needed for the immobilization, which is hard to find. But the method of physical adsorption is easy-to-implement and stable. That is why physical adsorption method was chosen for the immobilization of GOD (Section 2 in supplementary material).

3.3. Simulation of potential modulated LSPR

The simulation model was constructed by FDTD integrated development environment (Gedney, 2011). In the center of this model, the spherical structure represents an AuNP with a diameter of 40 nm, which is covered by PANI layer with a thickness of 20 nm based on the TEM images (Fig. S4). For bare AuNPs, the highest electromagnetic field intensity is on the surface of AuNPs with a relative intensity value about 3.0 (Fig. S5A). Compared to the nanocomposites, the highest electromagnetic field intensity is on the interface of AuNPs and PANI layer with a relative intensity value about 1.8 (Fig. 3A). The electromagnetic field distribution of the nanocomposites is relatively more uniform than that

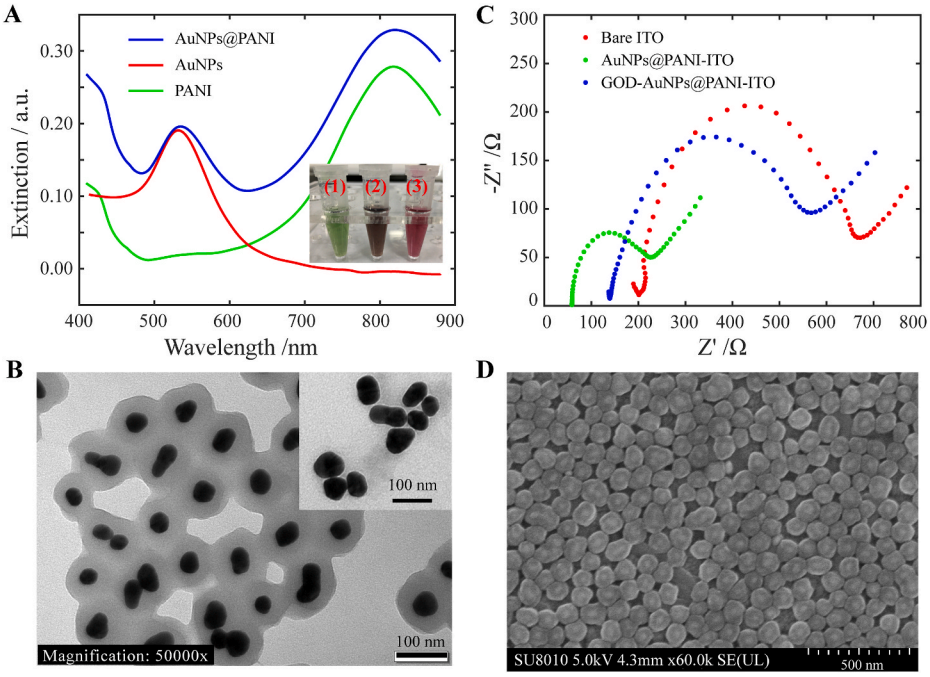

Fig. 2. The fabrication of LSPR chips. (A) The optical spectrum of AuNPs@PANI, AuNPs, and PANI (inset is aqueous solution of 1: PANI, 2: AuNPs@PANI, and 3: AuNPs). (B) The TEM image of nanocomposites shows that the AuNPs are coated by PANI layers (inset is TEM image of bare AuNPs). (C) The electrochemical impedance spectroscopy of each modification process. (D) The SEM image shows the morphological structure of the AuNPs@PANI modified LSPR chip.

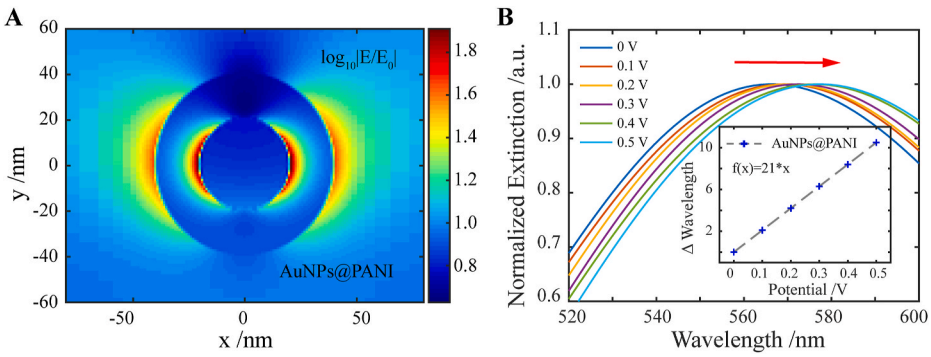

Fig. 3. Theoretical simulation of electric potential modulated LSPR based on AuNPs@PANI nanocomposites. (A) Electromagnetic field distribution of the nanocomposite indicates that the highest point of electromagnetic intensity is on the surface of AuNPs. (B) The quantitative simulation showed that the extinction peaks of nanocomposites were red shifted along with the increasing of applied electric potentials (inset is the linearity of optical extinction peak shifts).

of bare AuNPs, which means that the distribution of surface charge carriers is more susceptible to surrounding factors such as electric potentials. The electromagnetic field of nanocomposite coated ITO substrate was also calculated (Fig. S6), and the result illustrated that the effects of ITO layer on the electric potential modulation of plasmon resonance could be ignored. Quantitative calculations were performed for the nanocomposites with applied electric potentials ranged from 0 V to 0.5 V with an interval of 0.1 V, and the wavelengths of optical extinction peaks were red shifted for 10.5 nm (Fig. 3B). As showed in the inset of Fig. 3B, the peak shifts of the optical extinction were proportional to the applied electric potentials. Compared to the quantitative calculation for bare AuNPs (Fig. S5B), the response of nanocomposite to electric potential is greater.

Through the theoretical calculation and analysis, by coating with the conductive polymer, the nanocomposites exhibited excellent electric potential sensitivity on optical extinction peak shifts. Based on the Maxwell's equations and Lagrangian theory, the energy of electromagnetic field could be calculated by $E = hc/\lambda$ (E is energy, h is Planck constant, c is Lightspeed and λ is the wavelength of incident light), for which the energy is inversely proportional to wavelength (Aviles and Cervantes-Cota, 2017; Yee, 1966). Because of the enlarged gaps among the nanocomposites after the coating with PANI, the interactions among AuNPs were weakened which indicate the reduction in plasmon resonant energy. Thus, from the spectra, the optical extinction peaks of nanocomposites had a red shift compared with bare AuNPs which were consistent with the previous characterization results in Fig. 2A.

3.4. Electric potentials modulated LSPR

The nanocomposites modified LSPR chips were used to investigate the relationship between applied potentials and optical extinction peak shifts experimentally. While applying electric potentials on the LSPR chips, the optical extinction peaks were red shifted. As the applied potentials increased from 0 V to 0.6 V, the extinction peaks shifted about 11.4 nm (Fig. 4A). The significant responding of extinction peak shifts to electric potentials was calculated as 19.0 nm/V, indicating that small changes in electric potentials can be reflected in the extinction peak shifts (Fig. 4B). As comparison, the optical extinction peak of AuNPs modified LSPR chip was red shifted about 3.4 nm with electric potentials ranged from 0 V to 0.6 V (Fig. S7). The sensitivity of the extinction peak shifts to electric potentials was about 5.7 nm/V, which is weaker than that of the nanocomposites modified LSPR chip. Therefore, the plasmon resonance of the nanocomposites was more sensitive to electric potentials. Furthermore, the extinction peak changes of the nanocomposites modified LSPR chips were recorded five times at 0 V and 0.6 V, respectively (Fig. S8). The stable response showed good stability and reversibility of the potential modulations.

Due to the sensitivity of PANI to applied potentials, the extinction peak shifts of PANI coated AuNPs core-shell nanocomposites caused by electric potentials were significantly enlarged. After the nanocomposites were doped with protonic acid which decomposes into H^+ and counter anions, the degree of polymerization, conjugation effect, delocalized electrons of PANI molecular chain, and conductivity of PANI increased (Lu et al., 2017). When AuNPs were coated with PANI, the surface charge carriers of AuNPs were transferable to the PANI layer. Due to the influence of external electromagnetic field, the p-electron (also called pi electron) conjugated structure of PANI could occur a conjugation effect (Cui et al., 2018; Lin et al., 2021). Therefore, with increasing applied potentials, the density of free electrons and hot holes of AuNPs were more likely to enlarge, resulting in the increase of refractive index of

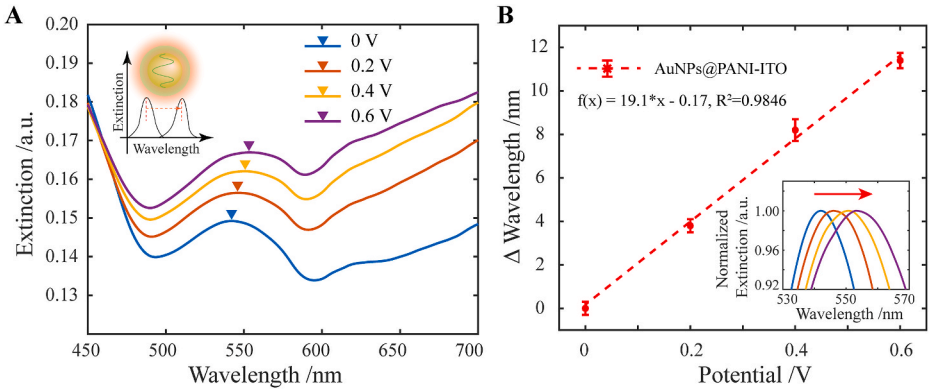

Fig. 4. The modulation of LSPR with electric potentials. (A) The optical extinction of AuNPs@PANI nanocomposite modified LSPR chips was modulated along with the applied potentials. (B) Shifts of optical extinction peaks for nanocomposites modified LSPR chip were linearly increased along with the increasing of applied potentials (inset is normalized enlarged view of the optical extinction peaks).

nanocomposites. Upon the increasing of refractive index, the optical extinction peaks were red shifted (Nishi et al., 2015). Thus, the degree of shifting of the optical extinction peaks increased along with applied electric potentials and the shifts were enlarged after the coating of PANI. These results were consistent with the theoretical calculations.

Theoretically, based on the relationship between extinction peak wavelengths and refractive index, and the relationship between applied potentials and refractive index (Mayer and Hafner, 2011; Ran et al., 2018), the extinction peaks of noble metal nanocomposites at certain applied potential can be determined. When electric potentials applied on the nanocomposites were changed from P_0 to P, the wavelength of extinction peak λ_P at potential P can be calculated through $\lambda_P = \lambda_{P_0}\sqrt{1+k(\Delta P)}$ ($\Delta P = P - P_0$ is the difference of applied potentials, k is a parameter only related to properties of the nanocomposites). On the macro level, the properties of nanocomposites are constant, therefore the extinction is changeable through ΔP. On the micro level, for the potential modulated LSPR, the distribution of hot holes and free electrons of the nanocomposites was susceptible to electromagnetic field generated by the applied potentials, indicating that the plasmon resonance can be modulated by applied potentials.

In noble metal, a plasmon is a collective oscillation of the free electrons (Sepúlveda et al., 2009). These plasmon oscillations could be treated as mechanical oscillations of the electron gas of a metal. The changes of free electrons are reflected in dielectric constant (Mejía-Salazar and Oliveira, 2018; Shen et al., 2019). When an external electric field was existed and applied on the nanocomposites, the free electrons changed their original position with the electromagnetic field generated by the applied voltages. That is, the free electron gas was displaced with respect to the fixed ionic cores. As the optical extinction is sensitive to the dielectric constant, the LSPR sensitivity is more related to the charge density of the nanocomposites.

3.5. Bio-electron transfer modulated LSPR

The nanocomposites modified LSPR chips immobilized with GOD were used for the modulation of LSPR via the bio-electron transfer of enzymatic catalysis. As the reaction proceeds, electrons are enriched on the chip and the open circuit potential is formed between electrodes. For LSPR chip without the immobilization of GOD, on the condition of 50 mmol/L glucose solution, the optical extinction peak was red shifted 1.4 nm (Fig. 5A). This is mainly due to the increase of solution refractive index caused by the increase of glucose concentration. Based on the GOD immobilized LSPR chip, on the condition of 50 mmol/L glucose solution, the extinction peak was shifted 4.1 nm (Fig. 5B), which was larger than the chip without GOD. The enlarged extinction peak shifts indicated that besides the influence of refractive index, the bioreaction of enzymatic catalysis also affected the extinction peak shifts. In this enzymatic catalysis bioreaction, electron transfers were the main factor that affected the optical extinction. Thus, in the presence of glucose, the optical extinction of GOD immobilized LSPR chip was modulated by the electron transfer of enzymatic catalyzing, where the optical extinction peak was red shifted along with the glucose concentrations (Fig. 5C). The normalized enlarged view of the optical extinction peaks of the GOD immobilized LSPR chip with different glucose concentrations was showed as inset in Fig. 5D. Their linearity was showed in Fig.5D, indicating that the red shift of extinction peak was approximate proportional to glucose concentration and can be used for glucose detection. Based on the calibration curve, this bio-electron transfer modulated LSPR sensing platform exhibits good reproducibility for the evaluation of glucose, and the limit of detection of glucose was calculated at about 5.63 mmol/L. As a proof of concept, with the pre-treatment process, this LSPR biosensing platform is potential for the detection of real samples, such as blood glucose or urine glucose, which is of great significance in the fields of disease diagnosis and health management.

Meanwhile, the optical extinction peak shifts of LSPR chips without the immobilization of GOD showed a slight red shift upon the increasing of glucose concentrations (Fig. S9A). The extinction peak shifts were caused by the refractive index changes of solution with the adding of glucose. Fig. S9B showed the linearity of extinction peak shifts along with the glucose concentrations. The reduced peak shifts compared to the optical extinction peak shifts of GOD immobilized LSPR chip indicated that the peak shifts of GOD immobilized LSPR chip were mainly caused by the bio-electron transfer of the enzymatic catalysis reaction. In certain ranges, as the concentrations of glucose increased from 10 mmol/L to 50 mmol/L, the electron transfers were strengthened, resulting in the increase of open circuit potentials from 0.048 V to 0.311 V (Fig. 5E). The linearity was showed as blue line in Fig. 5F. Different from the directly applied electric potentials, the enzymatic catalysis induced electric potentials were generated from inner of the bioreactions. Without the need of extra devices, the electron transfers captured by the LSPR chips were controllable through the intensity of bioreactions.

On the other hand, 4 mg/mL, 8 mg/mL, and 16 mg/mL GOD solution were prepared to evaluate the dependency between electron transfer efficiency and GOD concentration in chitosan. The results showed that, at low concentrations of GOD, the electron transfer efficiency was increased along with the concentration of GOD, whereas at high concentration, the increasing rate of electron transfer efficiency was slow down (section 3 in the supplementary material). Moreover, to evaluate

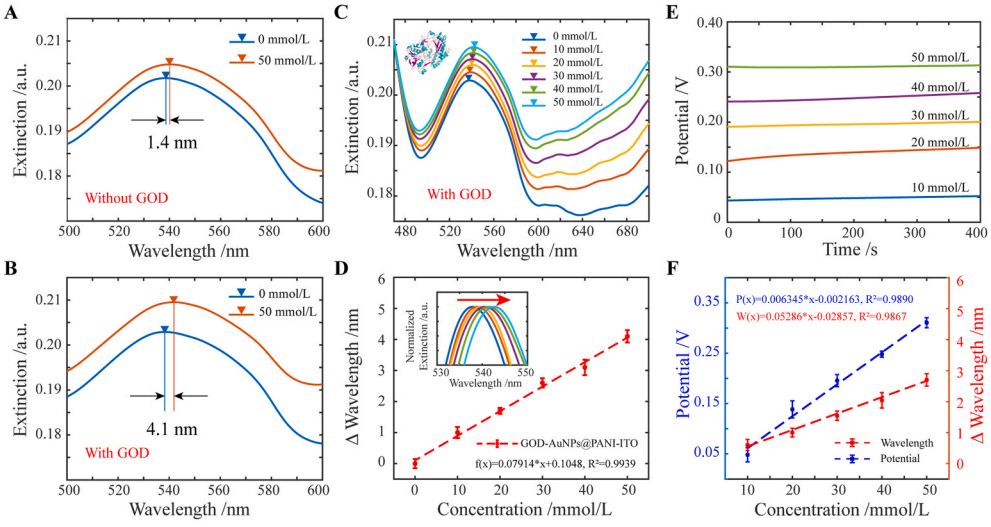

Fig. 5. Bio-electron transfer modulates the LSPR. With 50 mmol/L glucose solution, the optical extinction peak was shifted (A) 1.4 nm for LSPR chip without the immobilization of GOD and (B) 4.1 nm for LSPR chip with the immobilization of GOD. (C) Optical extinction spectra of GOD immobilized LSPR chips with different glucose concentrations. (D) Linearity of the extinction peak shifts along with glucose concentrations (inset is enlarged normalized view of extinction peaks). (E) Open circuit potentials of GOD immobilized LSPR chip with different glucose concentrations. (F) The linearity of open circuit potential with glucose concentrations (blue), and the linearity of extinction peak shifts with glucose concentrations excluding the influence of refractive index (red).

the selectivity of this biosensing platform, NaCl and sucrose solution with a concentration of 50 mmol/mL were tested under the same condition, and the LSPR chips with and without GOD were both utilized for the tests to match the situation of glucose detection. The results showed that the extinction peak shifts were sensitive to the substrate of glucose and barely have response to the solution of NaCl and sucrose, meaning the biosensing platform has selectivity with the enzymatic substrate of glucose (section 4 in the supplementary material).

Corresponding to the enzymatic catalysis generated open circuit potentials which were changeable according to the glucose concentration, excluding the influence of refractive index caused by solution concentration changes, the red shifts of optical extinction still showed linearity along with glucose concentrations (red line in Fig. 5F). The shift of extinction peak was about 4.1 nm when the enzymatic catalysis generated potential was 0.311 V. The increasing rate of optical extinction peak shifts with the enzymatic catalysis generated potential was about 13.183 nm/V, and the increasing rate of the optical extinction peak shifts with the glucose concentrations was about 82 nm/mol/L. Therefore, small changes in bio-electron transfer of enzymatic catalysis leads an obvious extinction peak shift, and the bio-electron transfer modulation of LSPR is promising in the monitoring of electron transfers and the detection of bioreaction substances.

3.6. Biosensing with charge density monitoring

Based on the layered structure and the electrochemical impedance spectroscopy of LSPR chip immobilized with GOD, equivalent circuit was modelled for the calculation of the electrochemical parameters. Usually, Randle circuit can be used for the analysis of impedance spectrum with solution resistance (R_s), charge transfer resistance (R_{ct}), open Warburg impedance (W_o), and constant phase element (CPE), as shown in Fig. 6A. The R_s and W_o represent the bulk properties of electrolyte solution. The CPE and R_{ct} both depend on the dielectric constant and insulting features at the interface of electrode/electrolyte that were often affected by the property changes occurring at the electrode interface. The protein of GOD immobilized on the surface of LSPR chip and the PANI coated AuNPs nanocomposites both have resistance and capacitance properties. Therefore, their electrical properties can be treated as a resistance-capacitance parallel circuit on the chip surface. Through the fitting of electrochemical impedance spectroscopy, parameters of the equivalent circuit were obtained. As showed in Fig. 6B, the fitting curve was overlapped with the Nyquist plot, and the Bode plot of phase and magnitude were both calculated indicating the resistance and capacitance properties.

While the glucose was oxidized to gluconic acid, the electrons of the enzymatic catalysis were transferred to the surface of LSPR chip. The enrichment process of the bio-electron is equivalent to the charging of capacitance causing the changing of electron distribution and the increasing of charge density. Based on the detected open circuit potential, charge density of the LSPR chip was obtained with the definition of equivalent capacitance. With the linearity relationship of glucose concentration and open circuit potentials, and the linearity relationship of glucose concentration and extinction peak shifts, the relationship of open circuit potentials of the GOD modified LSPR chip and the extinction peak shifts was obtained. Afterwards, the charge density of the GOD modified LSPR chip was calculated along with the shifts of extinction peaks (Fig. 6C). Based on the calibration curve, this bio-electron transfer modulated LSPR sensing platform exhibits reproducibility for the detection of charge density, and the limit of detection was calculated at about 0.51 μC/cm^2.

Furthermore, based on the LSPR chip with multiple regions, four points were selected randomly and their charge densities were simulated with glucose concentration of 0 mmol/L, 40 mmol/L, 45 mmol/L, and 50 mmol/L (Fig. 6D). Taking region 1 as reference point, based on the bio-electron transfer modulated LSPR mechanism, the charge densities of the other three regions are calculated as 13.4880 μC/cm^2, 15.1896 μC/cm^2, and 16.4658 μC/cm^2, respectively. With the relationship of charge density and extinction peak shifts of the LSPR chip, and the

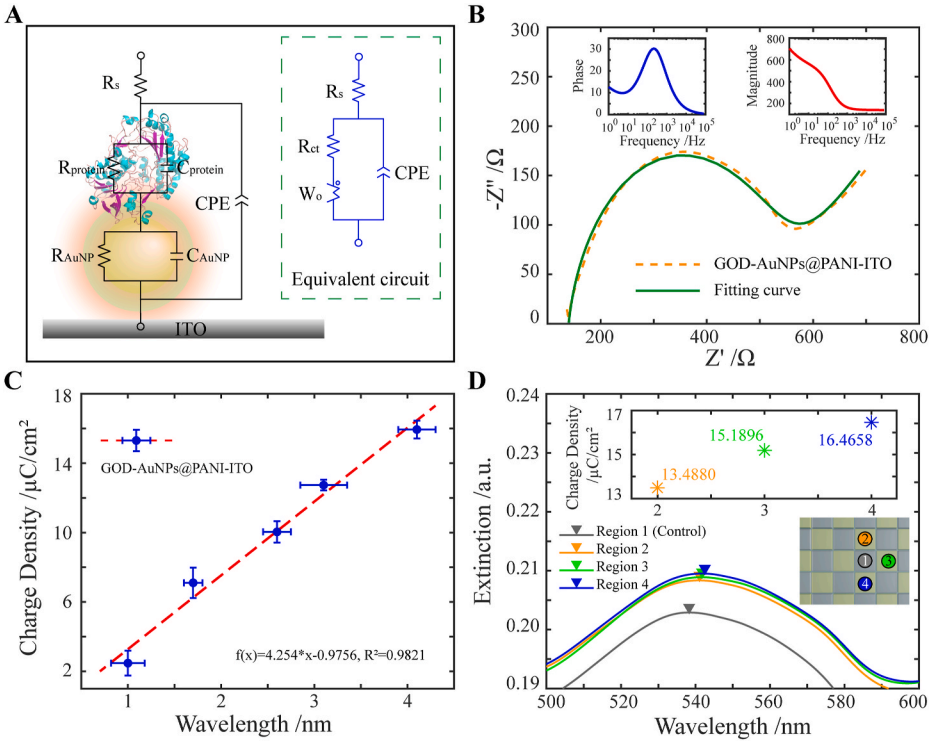

Fig. 6. Equivalent circuit fitting and charge density detection. (A) Equivalent circuit of the LSPR chip. (B) The Nyquist diagram and equivalent circuit fitting of the LSPR chip (insets are Bode plots of the equivalent circuit). (C) The calculated charge density of the LSPR chip along with the optical extinction peak shifts. (D) The detection of spatial charge density at different regions of the LSPR chip.

relationship of glucose concentration and extinction peak shifts of the LSPR chip, the corresponding glucose concentrations at these three regions were calculated as 40.958 mmol/L, 46.125 mmol/L, and 50.000 mmol/L, respectively. The detection results are very similar to the actual concentration of glucose, and the errors are within 2.5% indicating the high accuracy of this bio-electron transfer modulated LSPR biosensing platform. With the multiple region LSPR chip, this bio-electron transfer modulated LSPR platform enabled the detection of spatial charge density and the evaluation of substances involved correspondingly.

In our study, bioreaction of enzymatic catalysis with electron transfer was used for the simplified modulation process. Based on the bio-electron transfer modulated LSPR, the application of LSPR biosensing was expanded with the monitoring of spatial charge density. Bio-electron transfer are existed in most of the life activities, such as, the electron transfers of DNA crosslink, antigen-antibody reaction, bacterial metabolism, and so on (Kelley et al., 1999; Mishra et al., 2019; Wu et al., 2010). The extracellular electron transfer chain of bacterial metabolism reactions is related to the metabolic equivalent level (METS) (Light et al., 2018), through the bio-electron transfer modulated LSPR platform, the reaction substance at specific position could be detected for the accurately evaluation of bacterial metabolism. Furthermore, the spatial resolution of cell metabolites is very important for the research of life science (Pirbadian et al., 2020), based on the bio-electron transfer modulated LSPR, the spatial detection of cell metabolites can be greatly promoted. Since the mechanism of this bio-electron transfer modulation is energy-free and has no influence on the chips and reaction systems, this electricity of bioreactions modulated LSPR can also realize successive charge density monitoring and analytes evaluation for enzymatic catalysis, metabolism, or other life activities.

4. Conclusion

In summary, we have studied the bio-electron transfer modulation of LSPR, and constructed the LSPR biosensing platform with charge density monitoring. With the coating of PANI on AuNPs, the sensitivity of optical extinction to electric potentials was enhanced, which was consistent with the theoretical calculation. Based on the GOD immobilized LSPR chip, optical extinction of the nanocomposites was modulated by the bio-electron transfers of GOD catalyzing glucose. Through the electrochemical impedance spectroscopy equivalent circuit fitting, charge density of the LSPR chip was obtained with optical extinction peak shifts. With the multiple region LSPR chip, this bio-electron transfer modulated LSPR provides a promising approach for the detection of spatial charge densities and the evaluation of bioreaction substances at different position of the chip/solution interface.

Declaration of competing interest

The authors declare that they have no known competing financial interests or personal relationships that could have appeared to influence the work reported in this paper.

Acknowledgment

This work was supported by the National Natural Science Foundation of China (grant numbers 81801793, 81971703, 31671007), the China Postdoctoral Science Foundation (grant numbers 2018M630677, 2019T120518), the National Key Research and Development Program (grant number 2018YFC1707701), the Zhejiang Provincial Natural Science Foundation of China (grant number LZ18C100001), the Fundamental Research Funds for the Central Universities (grant numbers 2021QNA5018, 2021FZZX002-05) and the Collaborative Innovation Center of Traditional Chinese Medicine Health Management of Fujian province of China.

Appendix A. Supplementary data

Supplementary data to this article can be found online at https://doi.org/10.1016/j.bios.2021.113956.

References

Aviles, A., Cervantes-Cota, J.L., 2017. Lagrangian perturbation theory for modified gravity. Phys. Rev. D 96. https://doi.org/10.1103/PhysRevD.96.123526.
Boisselier, E., Astruc, D., 2009. Gold nanoparticles in nanomedicine: preparations, imaging, diagnostics, therapies and toxicity. Chem. Soc. Rev. 38, 1759–1782. https://doi.org/10.1039/b806051g.
Cortie, M.B., McDonagh, A.M., 2011. Synthesis and optical properties of hybrid and alloy plasmonic nanoparticles. Chem. Rev. 111, 3713–3735. https://doi.org/10.1021/cr1002529.
Cui, C., Faraji, N., Lauto, A., Travaglini, L., Tonkin, J., Mahns, D., Humphrey, E., Terracciano, C., Gooding, J.J., Seidel, J., Mawad, D., 2018. A flexible polyaniline-based bioelectronic patch. Biomater. Sci. 6, 493–500. https://doi.org/10.1039/c7bm00880e.
Freguia, S., Virdis, B., Harnisch, F., Keller, J., 2012. Bioelectrochemical systems: microbial versus enzymatic catalysis. Electrochim. Acta 82, 165–174. https://doi.org/10.1016/j.electacta.2012.03.014.
Gedney, S.D., 2011. Introduction to the finite-difference time-domain (FDTD) method for electromagnetics. Synth. Lect. Comput. Electromagn. 27, 1–250. https://doi.org/10.2200/S00316ED1V01Y201012CEM027.
Helmersson, U., Lattemann, M., Bohlmark, J., Ehiasarian, A.P., Gudmundsson, J.T., 2006. Ionized physical vapor deposition (IPVD): a review of technology and applications. Thin Solid Films 513, 1–24. https://doi.org/10.1016/j.tsf.2006.03.033.
Jackman, J.A., Rahim Ferhan, A., Cho, N.J., 2017. Nanoplasmonic sensors for biointerfacial science. Chem. Soc. Rev. 46, 3615–3660. https://doi.org/10.1039/c6cs00494f.
Jeon, J.W., Ledin, P.A., Geldmeier, J.A., Ponder, J.F., Mahmoud, M.A., El-Sayed, M., Reynolds, J.R., Tsukruk, V.V., 2016. Electrically controlled plasmonic behavior of gold Nanocube@Polyaniline nanostructures: transparent plasmonic aggregates. Chem. Mater. 28, 2868–2881. https://doi.org/10.1021/acs.chemmater.6b00882.
Kelley, S.O., Jackson, N.M., Hill, M.G., Barton, J.K., 1999. Long-range electron transfer through DNA films. Angew. Chem. Int. Ed. 38, 941–945. https://doi.org/10.1002/(SICI)1521-3773(19990401)38:7<941::AID-ANIE941>3.0.CO;2-7.
Kitajima, Y., Sakamoto, H., Ueno, K., 2021. Coupled plasmonic systems: controlling the plasmon dynamics and spectral modulations for molecular detection. Nanoscale 13, 5187–5201. https://doi.org/10.1039/d0nr06681h.
Li, S., Liu, J., Lu, Y., Zhu, L., Li, C., Hu, L., Li, J., Jiang, J., Low, S., Liu, Q., 2018. Mutual promotion of electrochemical-localized surface plasmon resonance on nanochip for sensitive sialic acid detection. Biosens. Bioelectron. 117, 32–39. https://doi.org/10.1016/j.bios.2018.05.062.
Light, S.H., Su, L., Rivera-Lugo, R., Cornejo, J.A., Louie, A., Iavarone, A.T., Ajo-Franklin, C.M., Portnoy, D.A., 2018. A flavin-based extracellular electron transfer mechanism in diverse Gram-positive bacteria. Nature 562, 140–157. https://doi.org/10.1038/s41586-018-0498-z.
Lin, C.W., Xue, S., Ji, C., Huang, S.C., Tung, V., Kaner, R.B., 2021. Conducting polyaniline for antifouling ultrafiltration membranes: solutions and challenges. Nano Lett. 21, 3699–3707. https://doi.org/10.1021/acs.nanolett.1c00968.
Loiseau, A., Zhang, L., Hu, D., Salmain, M., Mazouzi, Y., Flack, R., Liedberg, B., Boujday, S., 2019. Core-shell gold/silver nanoparticles for localized surface plasmon resonance-based Naked-eye toxin biosensing. ACS Appl. Mater. Interfaces 11, 46462–46471. https://doi.org/10.1021/acsami.9b14980.
Lu, W., Jiang, N., Wang, J., 2017. Active electrochemical plasmonic switching on polyaniline-coated gold Nanocrystals. Adv. Mater. 29, 1604862. https://doi.org/10.1002/adma.201604862.
Mano, N., 2019. Engineering glucose oxidase for bioelectrochemical applications. Bioelectrochemistry 128, 218–240. https://doi.org/10.1016/j.bioelechem.2019.04.015.
Mayer, K.M., Hafner, J.H., 2011. Localized surface plasmon resonance sensors. Chem. Rev. 111, 3828–3857. https://doi.org/10.1021/cr100313v.
Mejía-Salazar, J.R., Oliveira, O.N., 2018. Plasmonic Biosensing. Chem. Rev. 118, 10617–10625. https://doi.org/10.1021/acs.chemrev.8b00359.
Mishra, S., Pirbadian, S., Mondal, A.K., El-Naggar, M.Y., Naaman, R., 2019. Spin-Dependent electron transport through bacterial cell surface multiheme electron conduits. J. Am. Chem. Soc. 141, 19198–19202. https://doi.org/10.1021/jacs.9b09262.
Nehl, C.L., Hafner, J.H., 2008. Shape-dependent plasmon resonances of gold nanoparticles. J. Mater. Chem. 18, 2415–2419. https://doi.org/10.1039/b714950f.
Nishi, H., Hiroya, S., Tatsuma, T., 2015. Potential-Scanning localized surface plasmon resonance sensor. ACS Nano 9, 6214–6221. https://doi.org/10.1021/acsnano.5b01577.
Pirbadian, S., Chavez, M.S., El-Naggar, M.Y., 2020. Spatiotemporal mapping of bacterial membrane potential responses to extracellular electron transfer. Proc. Natl. Acad. Sci. U. S. A 117, 20171–20179. https://doi.org/10.1073/PNAS.2000802117.
Ran, L., Tao, Y., Guo, K., Shen, F., Zhou, H., Sun, Y., Zhang, R., Zhou, Q., Yang, J., Yin, Z., Guo, Z., 2018. Bias-scanning based tunable LSPR sensor. Phys. Chem. Chem. Phys. 20, 2146–2150. https://doi.org/10.1039/c7cp07565k.

Sepúlveda, B., Angelomé, P.C., Lechuga, L.M., Liz-Marzán, L.M., 2009. LSPR-based nanobiosensors. Nano Today 4, 244–251. https://doi.org/10.1016/j.nantod.2009.04.001.

Shen, Y., Chen, H., Xu, N., Xing, Y., Wang, H., Zhan, R., Gong, L., Wen, J., Zhuang, C., Chen, X., Wang, X., Zhang, Y., Liu, F., Chen, J., She, J., Deng, S., 2019. A plasmon-mediated electron emission process. ACS Nano. https://doi.org/10.1021/acsnano.8b08444.

Updike, S.J., Hicks, G.P., 1967. The enzyme electrode. Nature 214, 986–988. https://doi.org/10.1038/214986a0.

Wu, Y., Liu, S., He, L., 2010. Activators generated electron transfer for atom transfer radical polymerization for immunosensing. Biosens. Bioelectron. 26, 970–975. https://doi.org/10.1016/j.bios.2010.08.041.

Xu, G., Cheng, C., Liu, Z., Yuan, W., Wu, X., Lu, Y., Low, S.S., Liu, J., Zhu, L., Ji, D., Li, S., Chen, Z., Wang, L., Yang, Q., Cui, Z., Liu, Q., 2019. Battery-free and wireless epidermal electrochemical system with all-printed stretchable electrode array for multiplexed in situ sweat analysis. Adv. Mater. Technol. 4, 1–13. https://doi.org/10.1002/admt.201800658.

Xu, T., Geng, Z., 2021. Strategies to improve performances of LSPR biosensing: structure, materials, and interface modification. Biosens. Bioelectron. 174 https://doi.org/10.1016/j.bios.2020.112850.

Yee, K.S., 1966. Numerical solution of initial boundary value problems involving Maxwell's equations in isotropic media. IEEE Trans. Antenn. Propag. 14, 302–307. https://doi.org/10.1109/TAP.1966.1138693.

Zhang, D., Lu, Y., Jiang, J., Zhang, Q., Yao, Y., Wang, P., Chen, B., Cheng, Q., Liu, G.L., Liu, Q., 2015. Nanoplasmonic biosensor: coupling electrochemistry to localized surface plasmon resonance spectroscopy on nanocup arrays. Biosens. Bioelectron. 67, 237–242. https://doi.org/10.1016/j.bios.2014.08.022.

Zhong, R., Tang, Q., Wang, S., Zhang, H., Zhang, F., Xiao, M., Man, T., Qu, X., Li, L., Zhang, W., Pei, H., 2018. Self-assembly of enzyme-like Nanofibrous G-molecular hydrogel for printed flexible electrochemical sensors. Adv. Mater. 30, 1706887. https://doi.org/10.1002/adma.201706887.